C_{60} and C_{70} fullerenes and potassium fullerides

P. J. Benning, D. M. Poirier, T. R. Ohno, Y. Chen, M. B. Jost, F. Stepniak, G. H. Kroll, and J. H. Weaver
Department of Materials Science and Chemical Engineering, University of Minnesota, Minneapolis, Minnesota 55455

J. Fure and R. E. Smalley
Rice Quantum Institute and Departments of Chemistry and Physics, Rice University, Houston, Texas 77251
(Received 1 October 1991)

Photoemission and inverse photoemission studies of thin films of C_{60} and C_{70} reveal the distribution of occupied and empty electronic states of these molecular solids. X-ray photoemission results also show the C 1*s* main line and features related to π-π^* shakeups, electron energy losses, and plasmons. Potassium doping produces changes that can be related to the occupation of states derived from the lowest unoccupied molecular orbitals of the fullerenes and band-structure effects. Important differences are observed upon K doping of C_{60} and C_{70}, particularly in states near the Fermi level, and these would be reflected in the electron-phonon coupling, superconductivity, and the phase diagram. Resistivity measurements for K_xC_{60} show a resistivity minimum for K_3C_{60} and a dependence on stoichiometry that is indicative of dispersed conducting micrograins in an insulating medium. Oxygen-exposure studies demonstrate that K_xC_{60} thin films are unstable.

I. INTRODUCTION

The discovery of the carbon-cage fullerenes[1] and the development of techniques[2] for producing sizable quantities of them have led to intense scientific inquiry into the properties of fullerenes, fullerites, and fullerides. The report of conductivity[3] and then superconductivity[4–6] in C_{60} films containing alkali-metal atoms raised questions about the electronic states of the fullerites and the effects of doping. Photoemission studies[7–10] of K_xC_{60} addressed those questions and showed the filling of bands derived from the threefold-degenerate t_{1u} molecular levels. Detailed structural studies have shown that the superconducting phases have the stoichiometry K_3C_{60}.[6,11–14] They have also shown that alkali-metal incorporation produces K_4C_{60} and K_6C_{60} phases. Superconductivity has been observed for many solid solutions derived from C_{60} and the alkali metals.[4–6,15,16] Superconductivity has not been reported in any C_{70}-based fulleride, but there has been no explanation of its absence based on the electron energy spectrum.

This paper examines the properties of thin films of C_{60} and C_{70} before and after exposure to K. The experimental techniques include photoemission, inverse photoemission, and resistivity measurements. Spectroscopic analysis shows the molecular character of the fullerenes while revealing the quasiparticle spectrum and band gap. Core-level studies for C_{60} and C_{70} also show π-π^* excitation features, energy-loss features, and molecular plasmon losses. For both K_xC_{60} and K_xC_{70}, the combination of photoemission and inverse photoemission shows the disappearance of emission in the empty-state spectrum and its appearance in the occupied-state spectrum. Moreover, important differences are evident in the energy-level spectra of the two fullerides that would be reflected in electron-phonon coupling and superconductivity.

In this paper, we also present a model of fullerene film morphologies and changes wrought by alkali-metal incorporation. Analysis of the photoemission core-level results for K_xC_{60} shows phase separation for off-stoichiometric alkali-metal concentrations. Parallel resistivity measurements for K_xC_{60} films correlate electronic structure[7,8] with transport properties and show that the sticking coefficient for K adatoms is sensitive to the K concentration. Studies involving fulleride exposure to oxygen demonstrate the formation of K_2O_2 and KO_2-like surface species.

II. EXPERIMENT

Phase pure powders of C_{60} and C_{70} were separated by toluene extraction and liquid chromatography from the soot produced by arc discharge.[17] The fullerenes were sublimed from Ta boats that were resistively heated to $\sim$550 °C in ultrahigh vacuum. They were then condensed on clean substrates located $\sim$8 cm away. The sources were outgassed for $\sim$1 h at $\sim$500 °C before film growth was initiated. This made it possible to grow the fullerite films while maintaining chamber pressures below 1×10^{-9} Torr. In general, the substrates were held at 300 K, but growth was also done at 400 K and other investigations involved growth at 300 K followed by annealing at 450 K. In one case, C_{60} was deposited on a potassium film at 25 K and warmed to 300 K. Fullerene film thicknesses were measured with a quartz crystal thickness monitor using a density of 1.65 g/cm^3. The alkali metals were sublimed from commercial SAES getter sources. These sources were degassed over a $\sim$12 h period, always keeping the pressure below 1×10^{-9} Torr.

In this way, alkali-metal deposition onto the fullerite films could be done at $\sim 2\times 10^{-10}$ Torr. Procedurally, the substrates were prepared after the sources were degassed, the fullerenes were condensed and characterized with photoemission or inverse photoemission, and the samples were then exposed to the alkali-metal flux. Stable deposition rates were established prior to exposure to the alkali-metal source. Cleaved GaAs(110) crystals, silica glass, and thin films of K and Ti were used as substrates. For the transport measurements, contacts to the silica were made by depositing 1000-Å pads of Ti that left 1×1 cm^2 areas exposed. Copper wires were attached to the pads with silver epoxy, and an electrometer was used for resistance measurements.

The experiments were done in three different spectrometers. The synchrotron radiation studies were conducted at the Wisconsin Synchrotron Radiation Center using the Minnesota-Argonne monochromator and beamline. Photoelectrons were energy analyzed with a double-pass cylindrical mirror analyzer. The overall resolution was 400 meV for the valence-band spectra shown here. Higher-resolution studies (250 meV) conducted at 300 and 25 K revealed no additional structure. For the inverse photoemission studies, monoenergetic electrons of energy E_i were focused onto the sample surface and the energy distribution of the emitted photons was measured. This process corresponds to the radiative decay of electrons from states at energy E_i to lower-lying empty states. The photons were dispersed with a grating and were detected with a position-sensitive resistive anode detector. The overall resolution was ~ 400 meV. The x-ray photoemission studies used monochromatic Al $K\alpha$ photons ($h\nu = 1486.6$ eV, resolution ~ 600 meV). Closed-cycle He refrigerators were used in conjunction with W filament heaters to allow continuous variation of sample temperature from 25 to 475 K. Sample temperatures were measured with AuFe/chromel thermocouples mounted on sample holders. Oxygen dosing was done at 300 K. Parallel studies of thin film growth morphologies using scanning tunneling microscopy, STM, were done in another system by Li *et al.*[18] with comparable preparation conditions.

III. STRUCTURE OF FULLERENE THIN FILMS

Scanning tunneling microscopy studies of C_{60} and C_{70} thin films grown by vapor condensation have revealed surface morphologies that were remarkably complicated for a solid derived from spherical molecules bound by van der Waals forces.[18] One might have expected close-packed (111) surfaces and, indeed, the STM images did show such (111) domains. Intriguingly, growth at 300 K also produced surfaces with close-packed domains mixed with areas characterized by facets with (311) and (211) surfaces, large- and small-angle grain boundaries, single height steps, and multilayer islands. The surfaces were stable against repeated scanning, although tip-induced modifications were occasionally observed in the regions of disorder.[18] The size of the (111) domains and their perfection could be enhanced by growth on heated substrates or by postdeposition annealing.[18]

Despite the complexity of the surface for vapor-deposited films, photoemission measurements from different laboratories have given indistinguishable results for C_{60} with account taken of resolution or photon energy.[7–10,19–23] (To our knowledge, ours are the only results for C_{70} films.[24]) This may be because photoemission averages over millimeter-square areas and imperfections are plentiful. Photoemission has shown the Fermi level to be ~ 2.3 eV above the center of the band derived from the highest molecular orbital (HOMO) of C_{60} in all cases except the work by Krummacher *et al.*[22] where it was placed ~ 1.1 eV from the HOMO band. Inverse photoemission results for C_{60} have shown E_F to fall 1.5 eV below the center of the LUMO-derived band.[25] These energy positions relative to E_F reflect quasiparticle screening and the molecular-solid character of the fullerenes, as discussed in Sec. VI. The insensitivity to surface and bulk imperfections indicates the absence of localized energy levels that produce Fermi-level pinning near the band edges. This is consistent with the closed-shell character of C_{60} and the largely molecular properties of fullerene-derived solids. Angle-resolved studies of C_{60} at temperatures below the fcc-sc (where sc denotes simple cubic) phase transformation at 249 K (Ref. 26) may reveal band dispersion but the Brillouin zone is small and the band masses near the critical points have been estimated to be $\sim 1.3m_e$, making such studies difficult.[27–29]

Although clean fullerene films give remarkably consistent photoemission results, films grown when the fullerene sources were not carefully outgassed exhibited spectral broadening and shifts by ~ 0.3 eV to higher binding energy. This reflects Fermi-level alignment with states near the bottom of the conduction band derived from the LUMO level of C_{60}. No such Fermi-level pinning has been observed near the HOMO level, consistent with the high ionization potential of the fullerenes. The incorporation of dilute amounts of K in C_{60} also produced rigid spectral shifts and pinning of E_F near the LUMO band minimum (Sec. VI).

Photoemission studies have revealed that first-layer C_{60} bonding to metal and semiconductor surfaces is more than simply van der Waals in character.[23] These C_{60} films establish the Fermi level of the substrate as the common energy reference rather than the vacuum level, and this requires the creation of a dipole layer to compensate for differences in work functions. Such dipoles reflect mixing of the empty π states of the molecules with states of the substrate, yielding a π resonance similar to that for CO on Ni.[30] For growth on n-type GaAs(110), the dipole involves ~ 0.02 electrons per molecule so that the energy levels of the fullerenes are not significantly perturbed.[23] In this case, the spectral features observed for condensed C_{60} monolayers are indistinguishable from those for multilayers. For growth on metal surfaces where more charge transfer is involved, a few layers are needed before the influence of the substrate is negligible, as judged by photoemission line shapes.[23] In the most severe case studied to date, C_{60} on a potassium film, substrate atoms are displaced into suitable sites of the C_{60} layers so that

ionic bonds can be formed with the overlayer, as discussed in Sec. VIII.

IV. MORPHOLOGY AND ELECTRONIC STATES FOR K IN C_{60} FILMS

Figure 1 depicts a C_{60} film at different stages of K incorporation. Grain boundaries and other structural irregularities are not shown.[18] This figure is presented so that we can discuss the film morphology and correlate the morphology with the spectroscopic results. It is presented first so that reference to it can be made as the experimental results are discussed. For the pure fullerene film, the Fermi level lies between the LUMO- and HOMO-derived bands (top right of Fig. 1). Exposure to K produces a dilute solid solution (α-C_{60}) when the amount is below the solubility limit and the film is in thermodynamic equilibrium. These K atoms form bonds with surrounding C_{60} molecules, establishing new energy levels derived mainly from the LUMO levels. As a result, they pin E_F close to the LUMO band, as sketched. Phase separation into α-C_{60} and K_3C_{60} occurs when the K concentration exceeds the solubility limit. The work by Fischer[31] and Fleming *et al.*[13] has shown the K_3C_{60} phase to be a line compound with very little composition variation, and Fischer[31] showed that the α-phase solid solution has a slightly expanded fcc unit cell.

The low solubility of K suggests that K_3C_{60} nucleation would occur preferentially at the surface, not in the interior of a single crystal of C_{60}. In thin film samples, imperfections provide channels for easy diffusion and sites for nucleation. The characterization by Hebard *et al.*[33] of films produced by vapor condensation suggests C_{60} grains of ~60 Å dimension. We speculate that the critical size of a stable K_3C_{60} nucleus will be small because of the substantial energy gain per K atom associated with the higher ionization states of C_{60}. Calculations have indicated gains of 1.4 eV per atom for K in octahedral sites for K_2C_{60}, 1.4 eV per atom for K in tetrahedral sites of K_2C_{60}, and 1.7 eV per atom for occupancy of tetrahedral and octahedral sites in K_3C_{60}.[7,34] These energies are calculated relative to the standard states for K and C_{60}, and the K_1C_{60} and K_2C_{60} phases are hypothetical structures.

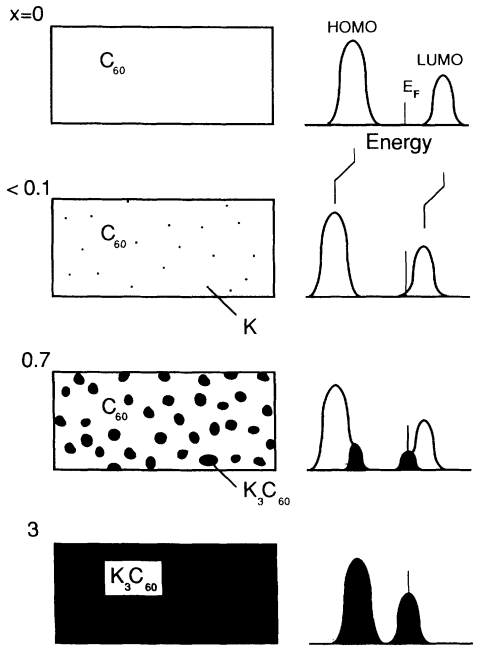

FIG. 1. Schematic of the morphology of a K_xC_{60} thin film. The positions of the HOMO- and LUMO-derived bands are shown in relation to E_F. For C_{60}, E_F lies near the middle of the gap. Dilute doping pins E_F near the edge of LUMO. Small K_3C_{60} grains nucleate, probably in grain boundaries or at imperfections in the film because of the low solubility of K in C_{60}. For K_3C_{60}, the Fermi level lies within the LUMO-derived band. Continued incorporation results in polycrystalline K_3C_{60}.

In Sec. VII, we argue that the condensation energy and the sticking coefficient for K atoms on C_{60} depends on the local structure of the surface. For deposition onto ordered C_{60}, the adatoms must form hybrid states with the LUMO levels if they are to supplement the van der Waals attraction to the surface. Once adsorbed, the atoms are able to diffuse on the surface or into the bulk, and the formation of K_3C_{60} nuclei will occur whenever the K concentration is sufficiently high. The richness of bulk diffusion channels and imperfections explains why resistivity results obtained immediately after K deposition represent homogeneous mixtures of K-C_{60} phases for films with thicknesses $\leq$2600 Å. For thick films or macroscopic crystals,[6,12,14,32] longer times are needed to reach equilibrium. Indeed, Kochanski *et al.*[32] found that it required ~400 sec to reach equilibrium conditions when a 4450-Å C_{60} film was exposed to K vapor at 300 K.

For fulleride growth by solid-state reaction with C_{60} powders and potassium metal, the surface layer is enriched relative to the interior with possible conversion to the bcc phase. This layer acts as a kinetic barrier so that thermal activation is needed for the formation of homogeneous macroscopic samples. In such solid-state reactions, the presence of oxides and other contaminants will also influence diffusion. Intermixing does not appear to be impeded for thin films exposed to an alkali-metal flux of K in ultrahigh vacuum with condensation rates of only $\sim 10^{14}$ cm^{-2} per minute. [The planar density of C_{60} (111) is $\sim 10^{14}$ cm^{-2}.] However, fulleride formation with other species can require annealing because of the larger activation energies for diffusion, even in thin films. This is certainly the case for Mg, Sr, Ba, and Yb.[35] In any case, fulleride formation will be driven by thermodynamics. Elements with large heats of formation and high ionization energies may form metallic clusters on fullerene films, as has been observed for Cr, Au, and Ti.[36]

The third panel of Fig. 1 depicts the formation of K_3C_{60} grains and grain growth. For two-phase samples, the spectral features of both phases will be present. There will also be broadening related to C_{60}-K_3C_{60} interface regions, although the ionic character suggests that the C_{60}-K_3C_{60} boundary will be sharp. This abruptness has been demonstrated by studies of C_{60} growth on K_3C_{60}.[10] Ultimately, the grains form a continuous film, as depicted in the bottom panel, with microstructures

that reflect the growth conditions and the structure of the starting film. Additional K incorporation produces nuclei of a body-centered-tetragonal (bct) K_4C_{60} phase.[13] The final K_6C_{60} phase has complete filling of the tetrahedral sites of the bcc C_{60} lattice, and each C_{60} is coordinated with 24 potassium ions.[14] Although this K_6C_{60} phase is insulating,[7,8,32] substoichiometric K_6C_{60} is characterized by Fermi-level pinning by holes near the top of the nearly filled LUMO band of the bcc compound. The Fermi level moves into the gap upon complete filling of those bands.

In our studies, the alkali-metal concentrations were determined from the emission intensities from the alkali metal and the fullerene, by the alkali-metal exposure times, and by line-shape analysis. In the x-ray photoelectron spectroscopy (XPS) studies, the C 1*s* and K 2*p* core-level intensities were used to determine the K concentration. (At $h\nu = 1486.6$ eV, the K 2*p* photoionization cross section is 2.38 times greater than that for the C 1*s*, and this is taken into account.[37]) The amount of K in the film was also measured by the attenuation of the substrate emission when the films were thin enough. In the synchrotron radiation photoemission studies, the intensities of the K 3*p* core levels and the LUMO-derived band were used to determine the alkali-metal concentration. In such studies, the intensities were compared to those for the saturated K_6C_{60} phase. The latter were easily determined because saturation to the insulating state resulted in an abrupt shift of the Fermi level. Further exposure led to emission from metallic clusters on the surface. Hence a film with the LUMO and core emission intensities half the size of those for K_6C_{60} was assigned a stoichiometry of K_3C_{60}. Line-shape analysis increased the accuracy of these procedures, and we estimate the uncertainty in x to be ± 0.2. For the inverse photoemission spectroscopy (IPES) studies, the concentration was determined by comparison of each spectrum to linear combinations of spectra believed to represent pure phases. We also considered the exposure time relative to that needed to produce the saturated film. This is a less reliable method because the sticking coefficient changes with K content, as discussed below, and the uncertainty is estimated to be ± 0.3.

For thin fulleride films, we expect the stoichiometry of the surface to be very nearly the same as the bulk stoichiometry because the fullerides are ionic materials with very high heats of formation.[7,34,38,39] In general, stoichiometries at the vacuum surface do not deviate from those of the bulk for ionic compounds, and surface relaxation or reconstruction is exceptional. For a vacuum-exposed K_3C_{60} (111) surface, the K atoms would be found in the surface-equivalent tetrahedral and octahedral sites, but not all of these sites would be occupied because of charge neutrality requirements. We cannot speculate about long-range ordering of the surface sites. We note that STM images for K_3C_{60} show ordered (111) surfaces in which only the C_{60} molecules are imaged.[18] Finally, Rutherford backscattering spectroscopy (RBS) measurements by Kochanski *et al.*,[32] taken together with this work, show that the minimum resistivity occurs for surface and bulk stoichiometries of $x = 3$.

V. C_{60} AND K-C_{60} CORE-LEVEL ANALYSIS

Figure 2 shows the C 1*s* and K 2*p* core-level energy distribution curves, EDC's, for K_xC_{60} formed at 300 K. The energy reference is the spectrometer Fermi level. The fullerene film was 4 monolayers (ML) (~ 30 Å) thick. Similar fulleride films formed with fewer C_{60} layers at 300 K or annealed to 400 K were spectroscopically indistinguishable. For the pure fullerenes, the spectrum of Fig. 2 gives a C 1*s* binding energy of 285.0 eV and a full width at half maximum (FWHM) of 0.65 eV. The latter is almost certainly limited by the resolution of the spectrometer.

The satellite structures, shown magnified by 10 in Fig. 2, are due to on-site and off-site π-π^* excitation processes and to plasmon losses. (On-site processes, as used here, are those that occur on the particular molecule from which the photoelectron is ejected.) This satellite region is expanded in Fig. 3 where the contribution from the main line has been subtracted and results from electron energy-loss (EELS) measurements are shown for comparison.[40,41] The first shakeup peak (feature 2), located 1.9 eV from the C 1*s* main line, is due to excitations from HOMO- to LUMO-derived states of the molecule that are induced by the creation of the core hole. This molecular HOMO-LUMO transition is monopole allowed ($\Delta l = 0$) and is likely to appear in a shakeup spectrum.[42] It is dipole forbidden in the isolated C_{60} molecule but solid-state effects mix the angular momentum quantum

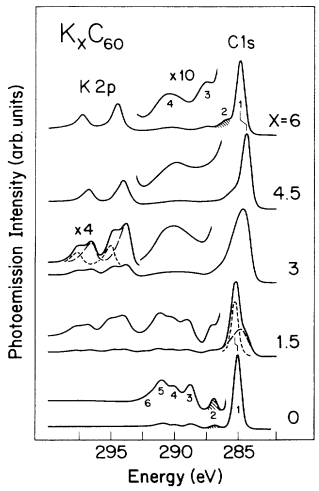

FIG. 2. C 1*s* and K 2*p* emission for a 30-Å K_xC_{60} film grown at 300 K. The bottom spectrum represents pure C_{60}. The middle spectrum represents metallic K_3C_{60} and shows a broad C 1*s* line with an asymmetry to higher binding energy. The top spectrum represents the insulating K_6C_{60} phase. The satellite structures labeled for K_0C_{60} and K_6C_{60} reflect contributions from on-site π-π^* excitations, off-site (dipole) energy losses, and plasmon losses. Feature 2 reflects an on-site HOMO-LUMO π-π^* excitation at 1.9 eV in C_{60} and 1.2 eV in K_6C_{60}. The C 1*s* main line for $K_{1.5}C_{60}$ includes contributions from lightly doped α-C_{60} and K_3C_{60}. The energy shifts identified by the vertical bars reflect those depicted in Fig. 1. The K 2*p* doublets reflect the inequivalence of the octahedral and tetrahedral sites.

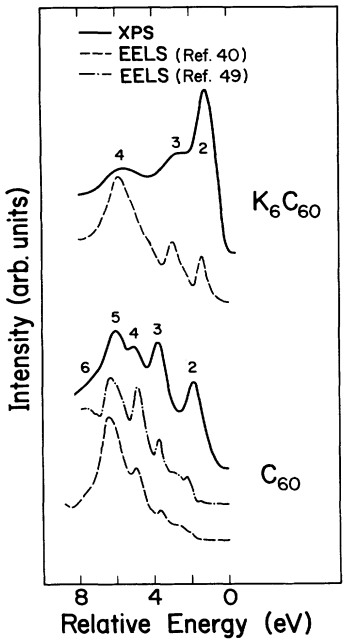

FIG. 3. C 1*s* satellite features, with the main line emission subtracted, compared to electron energy-loss spectra from Refs. 40 and 41. Structures 3–5 reflect dipole-allowed off-site energy losses, with underlying intensity from a π plasmon near ~ 6 eV and π-π^* monopole transitions. The feature at 1.9 eV in C_{60} represents the monopole-allowed HOMO-LUMO shakeup. The corresponding (dipole-allowed) feature at 1.2 eV in K_6C_{60} reflects a smaller gap.

number. Nonetheless, the transition is still weak in optical absorption[33,43–46] and EELS (Refs. 40, 41, and 47) where dipole selection rules are important. The satellite features at 3.7, 5.0, and 6.1 eV (labeled 3, 4, and 5) also originate from π-π^* transitions but their prominence in the EELS spectra[40,41] suggests that they are due to dipole-allowed transitions. Such excitations result in energy losses as the photoelectron propagates through the lattice. The interpretation in terms of dipole transitions is supported by the agreement between the optical conductivity derived from EELS data[48] and optical-absorption measurements.[33,43–45] The satellite feature labeled 3 appears anomalously strong when compared to the EELS data. Its strength is probably enhanced by contributions from monopole-allowed transitions involving HOMO-derived states and empty t_{1u}-derived states, both with $l=5$ symmetry as assigned in Refs. 29 and 46. The EELS experiments[41] indicate that the peak at ~ 6 eV results from both π-π^* transitions at 5.5 and 5.8 eV and the excitation of a π plasmon at 6.3 eV. The strength of the plasmon is dependent on the electron energy in EELS, as discussed by Gensterblum *et al.*[41] The shoulder labeled 6 in the shakeup spectrum is probably due to an underlying broad peak related to this collective oscillation. The satellite region is then composed of shakeup and inelastic loss features, an interpretation supported by the observation that such processes tend to overlap in the spectra from aromatic molecules.[42] C 1*s* spectra that extend to ~ 40 eV below the main line show a higher-energy plasmon at ~ 28 eV due to σ excitations.[21] This plasmon is observed in inverse photoemission[25] and EELS studies.[41,47,48] Additional monopole σ-σ^* transitions appear at 9.9 and 13.7 eV.[21]

The middle EDC in Fig. 2 was obtained with a K_3C_{60} film grown at 400 K. The broad C 1*s* main line (at 284.6 eV with FWHM of 1.5 eV) shows a pronounced asymmetry to higher binding energy and satellite features that are ill defined. Such spectral changes are indicative of the formation of the metallic phase for which the core-hole binding energy is reduced by metallic screening and photoelectron inelastic scattering produces a Doniach-Sunjic line-shape asymmetry. The broadening of the main line may reflect increased dissimilarity of the three symmetry-inequivalent C atoms in the K_3C_{60} structure. EELS spectra for $x \sim 3$ show a similar broadening of π-π^* transitions as well as low-energy intraband transitions between filled and empty portions of the LUMO-derived bands.[40] The π plasmon at ~ 6 eV persists although the π-π^* features are altered and washed out.

The K $2p_{3/2,1/2}$ core-level emission for K_3C_{60} appears as two spin-orbit-split pairs.[10] Their intensity ratio, 2 to 1, is derived from the number of tetrahedral and octahedral sites. The 1.1-eV energy separation represents a balance between initial-state effects (related to charge transfer and the crystal potential at the two sites) and photoemission final-state effects (related to the polarizability of the medium). Calculations for C_{60} have shown that the self-consistent-field potential at tetrahedral sites is ~ 1 eV deeper than at octahedral sites.[49] The (opposing) final-state shifts can be estimated by using the lattice dielectric properties.[50] In this case, K 2*p* holes in the smaller tetrahedral sites are better screened than those in the larger octahedral sites by ~ 2 eV, giving a net shift of ~ 1 eV to lower binding energy for K ions in tetrahedral sites relative to those in octahedral sites, as observed experimentally.

Figure 4 shows that the K 3*p* core-level emission appears as a single structure at ~ 18.3 eV. The FWHM was ~ 1.5 eV for K_3C_{60} and K_6C_{60}, showing the same broadening reported by Wertheim *et al.*[8] Spectral splitting due to population of tetrahedral and octahedral holes, as seen for the K 2*p* emission, is not observed for the K 3*p* levels. This indicates that the K 3*p* wave functions are extended enough that they overlap with orbitals of the surrounding fullerenes. This is particularly true for K in tetrahedral sites because the sites are smaller than the K^+ ionic radius. (The radius of the K^+ ion is controlled by the size of the 3*p* function.) Whereas the K 2*p* core-hole screening could be treated by simple polarization of a dielectric (because the relaxed final state did not overlap the fullerenes and the 3*p* shell was closed), the analogous treatment for a 3*p* core hole would be incorrect because charge transfer to the K 3*p* level is likely to occur in the photoemission final state. The breadth of the 3*p* emission for K_6C_{60} and its invariance in energy with x supports a picture of a more bandlike state. It should also be noted that the screening environment of the 3*p* electron in the initial state may be similar in K metal, K_3C_{60}, and K_6C_{60} because the charge that is transferred to the LUMO levels is still close to the K ion.

The top EDC of Fig. 2 shows the C 1*s* main line and satellite structures for K_6C_{60}. The energy shift is the result of E_F moving into the gap between the new HOMO-derived band and the new LUMO-derived band. (The distribution of such states is discussed in Sec. VI.) For K_6C_{60}, the K 2*p* line shape shows a single spin-orbit-split doublet, in agreement with structural studies showing a bcc lattice with K ions occupying a single type of slightly distorted tetrahedral sites.[14] The C 1*s* main line is again sharp (FWHM 0.77 eV) and new satellite features arise for molecules having fully occupied LUMO states. The lowest-energy transition is 1.2 eV from the main line (peak 2 in Figs. 2 and 3). This is in accord with the energy separation of the new HOMO and LUMO bands, as measured with inverse photoemission when both are unoccupied (see Fig. 5 below). The C 1*s* loss structure of Fig. 3 also reveals a broad shoulder at 3 eV and another feature at 5.8 eV. The EELS spectrum for K_6C_{60} contains peaks at these same energies although excitation cross sections appear to be quite different.

Figure 2 also shows C 1*s* and K 2*p* results for two-phase samples. Line-shape decomposition for $x=1.5$ reflects the superposition of contributions from C_{60} and K_3C_{60} (dashed lines). In this case, the C_{60} features are shifted by 0.25 eV because small amounts of K in the α-phase solution pin the Fermi level near the LUMO-derived band, as sketched in Fig. 1. The amounts of the two phases should be dictated by the lever rule, in agreement with spectroscopic results. The results for $x=4.5$ represent mixtures of K_4C_{60} and K_6C_{60}, according to the phase diagram,[13] but a unique line-shape decomposition is not possible because K_4C_{60} spectra have not been identified uniquely. However, the sharper main line from K_6C_{60} is evident and the K 2*p* feature appears as a single species with 2.7-eV spin-orbit splitting. This analysis of the K 2*p* results is consistent with the similarity of the tetrahedral sites for K_4C_{60} and K_6C_{60} but it is subject to improvement when single-phase K_4C_{60} samples are produced.

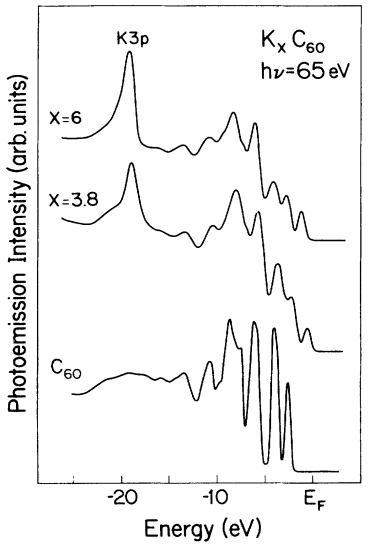

FIG. 4. Valence-band spectra for a 100-Å film of K_xC_{60} for $x=0$, 3.8, and 6. The wide valence bands exhibit sharp spectral features because of the high symmetry of the molecule. The leading two features are derived from π states, the features between -5 and -10 eV have mixed σ and π character, and the deeper features are σ derived. The center of the HOMO-derived feature is 2.25 eV below the spectrometer Fermi level, as measured by photoemission. Potassium addition results in emission from a new band at E_F that is derived from unoccupied bands of the fullerene. The top spectrum shows that the LUMO-derived feature shifts below E_F for insulating K_6C_{60}. Emission from the K 3*p* core is present as a broad peak 18.3 eV below E_F.

VI. C_{60} AND K-C_{60} VALENCE AND CONDUCTION BANDS

Figure 4 shows valence-band spectra for a 100-Å-thick film of C_{60} (bottom) and for K_xC_{60} for $x=3.8$ and 6.

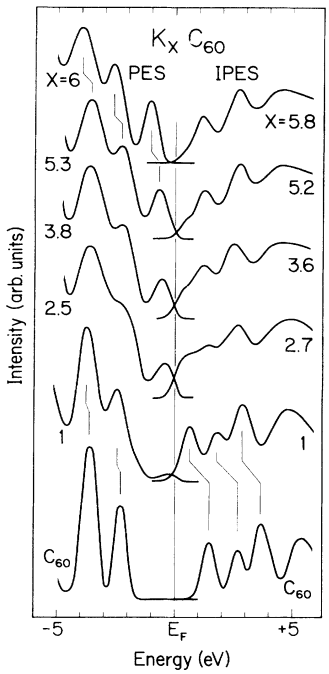

FIG. 5. Representative PES ($h\nu=65$ eV) and IPES ($E_i=17.25$ eV) spectra showing the effects of K incorporation. They were collected from 100- and 30-Å films. The normalization of the spectra is discussed in the text. K incorporation results in a 0.25-eV shift to lower energy of the PES features and a 0.75-eV shift to lower energy of the IPES features due to the movement of E_F to the edge of the LUMO bands and changes in screening in the doped film (compare to Fig. 1). The $x=1$ spectrum shows emission at E_F from phase-separated grains of K_3C_{60}. Adding K results in an increase of emission below E_F and a decrease of intensity above E_F as the higher stoichiometry phases grow. The top spectrum shows that E_F shifts into the gap when the LUMO bands are completely filled. The 2.6-eV separation of the HOMO-LUMO band edges in C_{60} represents the energy necessary to separate an electron and a hole in the solid. It should not be confused with the lower energy necessary to excite on-site molecular transitions.

These spectra were obtained with synchrotron radiation photoemission with $h\nu=65$ eV. At this energy, they emphasize the π states over the σ states[21] while showing growth of the K $3p$ emission at 18.3 eV. Additional valence-band spectra are shown in Fig. 5 to highlight features within 5 eV of E_F. Figure 5 also shows IPES spectra for a 30-Å film of C_{60} containing various amounts of K. The IPES spectra were obtained with an incident electron energy of 17.25 eV measured relative to the Fermi level. All of the spectra of Figs. 4 and 5 were referenced to the grounded spectrometer Fermi levels. The photoemission spectra were normalized to keep the HOMO intensity constant, and the IPES spectra were normalized to the height of the third feature. The two sets of data were then reconciled by setting the intensity of the LUMO feature in the IPES data to 3/5 the intensity of the HOMO feature for the pure fullerene film. This is the intensity ratio expected from the degeneracies of the two sets of π_u bands. Indeed, doping to $x=6$ yields this intensity ratio in the photoemission spectra. At the same time, neither photoemission nor inverse photoemission gives true density-of-states curves because both are affected by matrix element effects, as demonstrated in Ref. 51.

For C_{60}, the center of the HOMO-derived band is 2.25 eV below E_F. This position reflects the HOMO level in a C_{60} system where an electron has been removed by the photoemission process. The inverse photoemission results represent a system where an electron has been added to the molecular solid, and the center of the LUMO band is 1.5 eV above E_F. The experimentally observed energy separation between the centers of the HOMO and LUMO bands is then 3.75 eV. If the edges of the HOMO and LUMO bands are extrapolated to zero, we obtain a separation of 2.6 eV. For a conventional semiconductor, this extrapolation would give the band gap. The measured gap represents the energy needed to create an electron-hole pair and then separate them in the solid. It should not be confused with a molecular HOMO-LUMO excitation where the electron and the hole remain on the molecule, with or without extramolecular screening. We expect that extramolecular screening is small because the optical transitions for the molecule appear at 3.8, 4.8, and 5.9 eV for C_{60} in solution in hexane[52,53] (static dielectric constant 2.0) and 3.6, 4.6, and 5.6 eV for C_{60} in fullerene films[33,43–45] (static dielectric constant 4.4). Thus on-site HOMO-LUMO molecular excitations can account for weak optical absorption, but the electron and hole cannot be separated and they do not contribute to conductivity. The injection of an electron from a metal into a pure C_{60} film requires that the electron occupy a LUMO-derived state. The center of the LUMO band lies 1.5 eV above E_F, as measured by inverse photoemission, and the transport threshold should then correspond to injection at the leading edge of this band, i.e., ~ 1 eV. We note that the measurements of Hebard *et al.*[33] show the onset of dc conductivity at ~ 1 eV.

The molecular and solid-state origins of the occupied- and empty-state spectral features for C_{60} have been discussed elsewhere based on the calculated electronic state distribution.[21,25,29] In analysis of the experimental results, we assumed that all initial-state features were shifted relative to E_F by the same amount in the [$(n-1)$-electron] photoemission final state. We also assumed that all features in the [$(n+1)$-electron] inverse photoemission final state were shifted equally. Thus the creation of a quasiparticle in a molecular-orbital-derived state produces a rigid shift, regardless of the particular occupied or empty state. This assumption is supported by the fact that the wave functions are delocalized on the molecule and have similar spatial extents. Comparison to ground-state band calculations should then be correct to first order when energies are referenced to HOMO or LUMO. The breakdown of this approximation would introduce a state-specific energy reference. While this must be the case at some level of precision, the approximation appears to be sufficiently accurate that such things can be ignored. Although the calculations differ in the fine points, they provide a very good facsimile of the photoemission spectra,[27–29,54,55] agreement that supports the comparison of the quasiparticle spectrum to density functional calculations. Moreover, comparison of experimental solid-state results to calculations for isolated molecules[46,56] provides very good agreement when energies are referenced to HOMO or the vacuum level.

The first two occupied-state features for solid C_{60} (bottom curves of Figs. 4 and 5) are of π_u and π_g character with fivefold and ninefold degeneracy, respectively.[28,46,54–56] The experimental FWHM of the HOMO-derived band is 0.65 eV, consistent with band calculations that give a bandwidth of 0.58 eV.[49] The states are of mixed π and σ character for energies 5–10 eV below E_F (Fig. 4), and those below ~ 10 eV are σ derived. The overall valence-band width is very nearly the same as for graphite or diamond,[57] but the molecular symmetry of C_{60} assures sharp spectral features. In the empty states, the first two features are again π derived but analysis shows angular momentum mixing.[28,29] For this reason, the dipole selection rules that forbid HOMO-LUMO transitions are relaxed in the solid. Moreover, such selection rules would apply strictly only at the Brillouin-zone center where the angular momentum character is pure. For higher-energy states, the calculations show the onset of intermolecular interactions.[28,29] Indeed, the third empty-state peak of Fig. 5 contains substantial contributions from π states and states of nonmolecular origin.[25]

The valence- and conduction-band spectra in Figs. 4 and 5 provide evidence that filling of LUMO-derived bands with electrons donated from alkali-metal atoms does not result in simple rigid band shifts. This is particularly evident in the empty states because the separation between the LUMO+1 and LUMO+2 features (Fig. 5) changes from 1 eV in pure C_{60} to 1.3 eV in K_3C_{60} to 1.6 eV for K_6C_{60}. Since these states are empty and quasiparticle screening would not change their relative energies, the differences reflect a modification in the underlying density of states. Such effects are greatest for the extended empty states, particularly those near in energy to the K $4s$ band. The calculations indicate that the K $4s$ band lies above E_F in K_3C_{60} and mixes mostly with nonmolec-

ular states having appreciable amplitude at the interstitial sites.[34] There are no spectral features that distinguish it since it only adds one state to a feature already containing eight bands. The empty-state structure probed with x-ray absorption spectroscopy[9] and EELS (Ref. 38) shows similar development with K addition with slight differences in the relative positions of peaks that result from the presence of the core hole.

The decrease in peak height of the leading π features evident in Fig. 4 is a result of broadening. Measurements of the integrated intensities show that there is no reduction in emission form the leading features until $x \sim 5$ and then only HOMO-1 experiences a 20% reduction in emission. This is probably a result of changes in photoemission cross section due to final-state symmetry.[51]

The broadening observed in Figs. 4 and 5 is a combination of several processes. Changes associated with K doping are observed in the occupied-state spectra where the π-derived features shift 0.15 eV more (toward E_F) than the lower-lying σ-derived features upon transformation from C_{60} to K_3C_{60}. This explains the line-shape changes of the feature at 7 eV below E_F because it is derived from σ- and π-derived states and their relative positions within the feature change. In addition, there is structural disorder related to grain boundaries and imperfections and, hence, differences in local bonding configurations in the mixed-phase samples. The FWHM of the HOMO feature changes from 0.65 to 1.0 to 0.9 eV for C_{60}, K_3C_{60}, and K_6C_{60}. Changes in the width of the LUMO feature are even larger since the FWHM of the half filled LUMO band in K_3C_{60} is 1.1 eV compared to 0.75 eV for K_6C_{60}.[9]

To investigate the effect of dilute amounts of alkali-metal atoms in C_{60} films, we exposed C_{60} films of thicknesses between 16 and 2600 Å to produce stoichiometries below $K_{0.1}C_{60}$. Analysis showed a shift to higher binding energy by ~ 0.25 eV for the valence-band and C 1*s* features, as depicted in Fig. 1. In part, this reflects pinning of E_F near the LUMO band as states derived mainly from LUMO mixed with K 4*s* and were populated. At the same time, the empty-state features shifted 0.75 eV toward E_F. Hence the initial-state effects related to E_F level pinning are reduced by final-state effects related to quasiparticle screening for photoemission and enhanced for inverse photoemission. While initial-state effects are the same for photoemission and inverse photoemission (to lower energy), the screening effects are in the opposite direction (toward E_F in both cases). The results demonstrate Fermi-level movement by 0.5 eV and a screening shift of magnitude 0.25 eV, assuming symmetric screening shifts for the occupied and empty states.

Figures 4 and 5 show that the LUMO band shifts 0.4 eV away from E_F when it is fully occupied at $x = 6$. This implies that the solid, defect ridden as it is, forms the local geometry needed to fill the LUMO-derived molecular states of C_{60}. Were this not the case, E_F would be pinned at the top of the LUMO band in a fashion equivalent to that just discussed for $K_{0.1}C_{60}$. The IPES spectra of Fig. 5 demonstrate such pinning for x slightly below 6. The Fermi-level shift at K_6C_{60} is difficult to observe with IPES since it is largely offset by the opposing screening shift. The fact that an insulating state is reached with E_F in the gap of the (new) molecular solid implies that structural imperfections do not introduce levels that can pin E_F near the band edges. No evidence was found for the filling of the LUMO$+1$ band upon further K exposure but the valence bands showed evidence for metallic K growth on the surface.

VII. K_xC_{60}, A GRANULAR METAL

Figure 6 summarizes the results of resistivity measurements done in conjunction with photoemission studies for a 2600-Å-thick C_{60} film exposed to a potassium flux at 300 K (area 1×1 cm^2). The resistivity was monitored continuously using a two-point method during K exposure, but exposure was interrupted so that photoemission spectra could be collected ($h\nu = 65$ eV). The solid line indicates the resistivity when the concentration was determined from the emission from the LUMO-derived bands and K 3*p* core level (estimated accuracy ± 0.2), with dots indicating the stoichiometries for which spectra were collected. While the two-point technique is vulnerable to contact resistance effects, the doping level in K_xC_{60} was high enough to produce an Ohmic contact for $x \geq 0.3$, and our analysis emphasizes these stoichiometries.

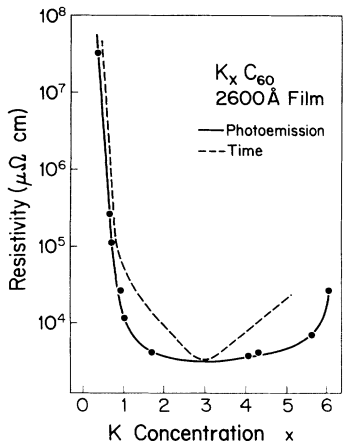

FIG. 6. The resistivity as a function of K concentration for a 2600-Å film of C_{60} prepared at 300 K. The dashed line represents the behavior when the concentration was determined by timed exposure to the source. The solid line shows the behavior where concentration was determined from photoemission intensities. The exposure time measurements overestimate the concentration for $x < 3$ and underestimate it for $x > 3$ because the sticking coefficient of K on K_xC_{60} varies with x. The resistivity minimum of 3200 $\mu\Omega$ cm occurs for K_3C_{60}. The resistivity behavior for low stoichiometries is indicative of a system with metallic grains growing in an insulating medium, consistent with phase separation of K_3C_{60} in C_{60} (see Fig. 1). Calculations based on a granular metal model gave a grain density of $\sim 10^{18}$ cm^{-3} and grain sizes of ~ 100 Å when coalescence starts near $x = 1$.

Indeed, a change in the probing current for representative stoichiometries showed no effects, i.e., no Schottky-like responses. Further, the resistivity behavior measured as a function of exposure time agreed quite well with that reported by Kochanski *et al.*[32] based on their four-point van der Pauw method.

The dashed line in Fig. 6 shows the resistivity for K_xC_{60} based on concentrations determined from exposure time to the K source. In this case, the resistivity minimum was assigned to the stoichiometry of K_3C_{60}. While the flux from the source is stable, the exposure time results are less reliable than the K concentrations determined by photoemission because the sticking coefficient changes with x. Figure 6 shows that the time interval needed to go from K_3C_{60} to K_6C_{60} is $\frac{2}{3}$ of that needed to reach K_3C_{60} from K_0C_{60}. Kochanski *et al.* have shown the same behavior for time exposures and they noted that it suggested an increased sticking coefficient with x. Such differences in sticking coefficient are reasonable since a K atom impinging on the surface forms ionic bonds that involve charge transfer to the LUMO levels. We speculate that the ionic bonds for low K-C_{60} coordination are not particularly favorable, based on the energetics calculated for K_1C_{60}.[34] Bonding and the sticking coefficient will be better once K_3C_{60} or the other unsaturated phases constitute the surface, based again on the energetics of K atoms in ordered bulk structures.[34] Such crude estimates imply that sticking on saturated K_6C_{60} surfaces is again less probable. Finally, we note that stoichiometry errors in the photoemission measurements would make the discrepancy larger, not smaller, because the surface is more likely to be richer in K than poorer.

In our resistivity studies, we found that the transport properties of the pure C_{60} films were sensitive to irradiation with visible light, 65-eV photons, and changes in temperature. Photon irradiation reduced the resistance on a <1 sec time scale. This is consistent with promotion of charge carriers into the conduction bands. Equivalent reductions were found upon annealing, and they probably reflect structural changes since there was incomplete recovery. However, the detailed behavior was sample dependent and quantitative conclusions cannot be made. The exposure of a pure C_{60} film to a hot filament also produced anomalous results with the resistance increasing briefly for some samples and decreasing immediately for others. No such effects were evident after the films were lightly doped ($x<0.1$). In all cases, the resistivity of even the lightly doped C_{60} films was greater than 5×10^8 $\mu\Omega$ cm.

The solid and dashed lines of Fig. 6 indicate that the resistivity decreases sharply for $x<1$. From the K concentration determined with photoemission, the resistivity is relatively unchanged between $x=1.5$ and ~5. This broad minimum is not evident when the stoichiometry is determined from exposure time (dashed line). Instead, the dependence on x is approximately exponential from $x=1$ to 3 and from 3 to 5, as shown by the nearly straight line on the log-linear plot in Fig. 6.

The gross features of the resistivity behavior can be understood by considering a granular metal model in which metallic K_3C_{60} grains are imbedded in an insulating C_{60} matrix.[58,59] In a granular metal model, the resistivity dependence on x can be separated into dielectric, transition, and metallic regions. In the dielectric region, conduction results from tunneling between metallic grains through the insulating medium. Hence the resistivity scales as $\exp[(N/x)^{1/3}]$ where N is the metallic grain density.[58] In the fully metallic region, the resistivity is determined by electron scattering. In the transition region, transport is accomplished by a combination of tunneling and metallic conduction. The number of direct pathways for conduction increases with K concentration. Hence the resistivity varies as $(x-x_c)^{-p}$ where x_c is the threshold composition between the metallic and dielectric regions and the exponent p varies between 1 and 2, depending on geometry used to model the morphology.[59]

The drop in resistivity for $x<1$ does not depend significantly on whether the K content is determined by time of exposure or photoemission signal since the concentration is low (Fig. 6). Calculations which model the system with spherical metallic K_3C_{60} grains on the lattice points of a simple cubic array growing in an insulating C_{60} medium give a grain density of $\sim10^{18}$ cm^{-3}. Indeed, the rapid resistivity decrease in this region guarantees a reasonable fit to the model despite the uncertainty in x. The calculations also predict that conduction pathways will form when $x\sim1$, corresponding to grains that are ~100 Å in diameter. Such grain sizes are similar in size to the grains in pure C_{60} films deduced from the x-ray diffraction analyses of Hebard *et al.*[33] and STM analyses of Li *et al.*[18] The leveling off of the resistivity where the K_xC_{60} grains form conduction pathways near $x=1$ is in agreement with the model calculations.

The approximate nucleation density and grain size reported here do not vary greatly with the geometry used to model the grain distribution within the film. The broad minimum in $\rho(x)$ suggests that the grain size is much larger than the scattering length of electrons in K_3C_{60}. This can be qualitatively understood by realizing that films with large grains have less insulator surface area and, hence, electron scattering relative to small grains with the same nominal stoichiometry. Enhanced scattering in films with small grains would produce a faster decrease in resistivity and hence a sharper minimum when x approaches 3 and the insulating C_{60} phase is consumed.

Kochanski *et al.* have examined the temperature dependence of the resistivity for K-C_{60}, finding activated conduction except when x was near 3. In their experiment, they determined the stoichiometry by the exposure time. As can be seen from Fig. 6, this contracts the range over which metallic behavior can be expected. When account is taken of the nonlinear sticking coefficient, their results would indicate that metallic conductivity would occur for concentrations as low as $x=1.3$. This would be in rough agreement with the granular metal model where $x_c=0.9$. This value of x corresponds to the separation between metallic and activated conduction.

Finally, our transport measurements show that the film

resistivity of K_3C_{60} decreases with film thickness up to ~ 1000 Å but then remained relatively constant (our thickest film was 5000 Å). This supports the conclusions of Ref. 32 in which a minimum resistivity was reported for thick films. Our resistivity value of 3200 $\mu\Omega$ cm for K_3C_{60} agrees within experimental uncertainty to reported values of 2000 (Ref. 3), 5000 (Ref. 4), and 2200 $\mu\Omega$ cm (Ref. 32).

Resistance measurements for a 2000-Å K_xC_{70} film showed a minimum resistivity of 4.5×10^5 $\mu\Omega$ cm, which is in excellent agreement with the conductivity maximum of 2 $S\,cm^{-1}$ reported in Ref. 3. Quantitative correlation between x and ρ was not obtained, so analysis similar to that for K_xC_{60} is not presented. Such analysis would be expected to show interesting differences between K_xC_{60} and K_xC_{70} since dissimilar phases appear to be present in the two systems (Sec. X).

VIII. C_{60} OVERLAYERS ON POTASSIUM

The ease of K diffusion through a C_{60} thin film lattice can be demonstrated by examining the reaction that accompanies C_{60} deposition onto K metal. To do this, we formed a $\sim$15-Å-thick K layer on GaAs(110) at 25 K. The thickness was estimated by comparison with the results for saturated coverages of K-GaAs(110), namely, 0.5–1 ML at 300 K (Ref. 60) and by attenuation of the GaAs substrate emission. The formation of a metallic potassium layer prior to C_{60} deposition was evident from the asymmetry of the K 2*p* core-level emission and the fact that a plasmon loss feature was observed for each core level. (Plasmon losses of $\sim$3 eV were also observed for photoelectrons arising from Ga and As excitation since they traversed the K layer.) The addition of submonolayer amounts of C_{60} at 25 K produced two effects. First, the plasmon losses disappeared, suggesting a change in electron distribution in the K film. Second, the emission from the GaAs substrate was attenuated more than the emission from the K layer, indicating the movement of K into the C_{60} layer. To account for these effects, we postulate that K atoms occupied interface sites that maximized their coordination with the C_{60} overlayer. This demonstrates that sites in the monolayer C_{60} islands[18] were energetically attractive and that ionic bonds could be formed. Analysis of the C 1*s* main line for the C_{60} on K supports this interpretation since it was only $\sim$0.2 eV narrower and at approximately the same binding energy as the metallic K_3C_{60} phase. Hence the mixing of K in the C_{60} monolayer results in the donation of charge to the adsorbed fullerenes. Since K has a small work function, the amount of charge donated, and hence the resulting interface dipole field, is large, causing K to move to interstitial sites.

The addition of C_{60} to form a layer $\sim$3 ML thick did not produce any significant K movement into the surface layers when the temperature was below 100 K. This was shown by the attenuation of the K and GaAs emission and the fact that the C 1*s* line shape was representative of a third C_{60} layer.[23] Once the electrostatic forces were balanced, therefore, intermixing was restricted at 25 K. Photoemission spectra taken over a period of $\sim$12 h showed minimal K outdiffusion. More extensive intermixing was observed when the kinetic constraints were relaxed by slowly warming. In particular, the K 2*p* emission increased when the sample was warmed to $\sim$100 K and the C_{60} overlayer was K saturated by the time the temperature reached $\sim$200 K, producing K_6C_{60}.

The K-C_{60} changes observed in the first layer at 25 K demonstrate that the release of atoms from the metallic K interface was not a limiting factor in intermixing. This suggests that we can model the temperature-dependent behavior with K diffusion through the interstices of the fullerite lattice. At 200 K, this diffusion through the $\sim$30-Å-thick layer forms the saturated phase in less than one hour. From these conditions, we conservatively estimate an activation energy for diffusion of $\sim$0.5 eV, assuming a typical jump frequency of 10^{13} sec^{-1}. The diffusivity calculated for room temperature based on this activation energy is very high. This supports the observations from our resistivity measurements in which we found no discernible lag in reaching the equilibrium resistance for 2600-Å films during K deposition at a rate of $\sim$1 Å/min at 300 K. This, too, is in agreement with the diffusivity value of 10^{-12} cm^2/sec estimated in Ref. 32.

IX. K-C_{60} OXIDATION

A critical issue related to the application of the K_xC_{60} phases concerns the instability when exposed to the atmosphere. To investigate such effects, we exposed a 30-Å film of K_6C_{60} to O_2 at 300 K. The top EDC of Fig. 2 represents the starting point and Fig. 7 summarizes the changes in the O 1*s*, C 1*s*, and K 2*p* spectral features as a function of O_2 dose. The spectra are normalized to acquisition time. Exposure to 2 L (1 L$=10^{-6}$ Torr sec) introduces a small O 1*s* feature at 530.8 eV as well as shifts in the C 1*s* and K 2*p* EDC's by 0.6 and 0.8 eV to lower binding energy. These shifts can be understood by recognizing that K previously bound in the fulleride lattice has been leached to react with oxygen. This reduces the K content in the fulleride so that it is no longer insulating K_6C_{60}. The observed shifts therefore represent the positioning of E_F in the LUMO band (compare to Figs. 2 and 5). The shift appears to be greater for K because there is a K-oxide component at lower binding energy. The dashed line for 10 L exposure emphasizes the oxide component. Intensity analysis showed that the K 2*p* emission increased as a result of oxygen exposure because K atoms were withdrawn from the fulleride to form the surface oxide. Potassium is then the moving species, consistent with a greater activation energy for O_2 diffusion through the fulleride and the low probability of oxide formation internally.

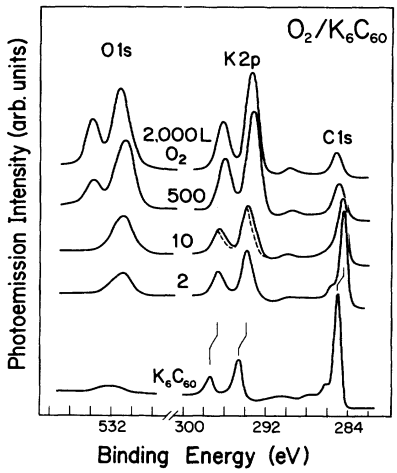

FIG. 7. Effects of exposing a 30-Å film of K_6C_{60} to O_2 at 300 K. The spectra are normalized to photon flux to emphasize intensity changes. The bottom spectrum is equivalent to that of Fig. 2 with a small oxygen signal. O_2 exposure produces emission at 530.8 eV and a shift of the K 2*p* and C 1*s* feature to lower binding energy because K_2O_2 forms at the surface and the fulleride stoichiometry is reduced. After 10 L exposure, a K-O feature appears in the K emission (dashed line). Continued exposure results in O-emission at 533.8 eV as a KO_2-like phase forms.

Figure 7 shows that the O 1*s* emission at 530.8 eV increased in intensity and a second feature formed at 533.8 eV by 500 L exposure. Comparison with the literature shows that the 530.8-eV peak corresponds to K_2O_2 and the second feature corresponds to KO_2.[61] Intensity analysis for the C 1*s* emission and for Ga and As emission from the substrate shows that the former decreased more rapidly, reflecting further surface segregation and oxidation of K. We note that studies of K_xC_{60} with low metal stoichiometries also demonstrated that oxygen exposure led to K loss. Such processes can be understood by recognizing that the heats of formation[62] of KO_2 and K_2O_2 are -3 and -2.6 eV/(K atom), respectively, compared to about -1 eV/(K atom) for the fulleride phases.[49]

The initial oxidation of K_6C_{60} is limited by the amount of O_2 impinging on the surface. K_2O_2 formation is favored when the supply of K is abundant. However, KO_2 forms when the K supply is the controlling parameter. This accounts for the change in the O 1*s* emission of Fig. 7. Simple oxygen exposure develops a K_2O_2 surface layer that impedes K diffusion. When the oxide layer formed by exposure to 2000 L O_2 was annealed to 120 °C without further O_2 exposure, the KO_2 peak disappeared. This reflects further K depletion and transformation of KO_2 to K_2O_2.

Finally, the relative stability of the fulleride phases was investigated by O_2 exposure of fullerides with compositions of $x=1.5$ and 3. For K_3C_{60}, an oxide layer appeared after 1000 L O_2 exposure, and its thickness was half of that formed on a K_6C_{60} film. Hence K_3C_{60} and K_6C_{60} were equally susceptible to oxidation, consistent with the heats of formation per K atom for the two fulleride phases. Similar O_2 exposures of a film with composition of ~ 1.5 showed little effect. This probably reflects the fact that O_2 does not diffuse readily into the film. In this sense, the C_{60} phase protects internal fulleride grains. As Kroll *et al.*[63] have shown, C_{60} molecules react with oxygen but only under rather severe conditions of O_2 and photon exposure.

An attempt was made to passivate a K_xC_{70} film with 5000 Å of CaF_2 so that the sample could be examined *ex situ*. The resistance was continuously monitored and showed no change upon CaF_2 deposition. Backfilling the vacuum chamber with ~ 1 atm of nitrogen caused the resistance to increase by a factor of ~ 2, presumably due to impurities in the N_2 or desorption from the chamber walls. Exposure to air resulted in a rapid resistance increase over several orders of magnitude, indicating that the CaF_2 buffer was insufficient to prevent oxidation of the K in the K_xC_{70} film.

X. C_{70} AND K-C_{70}

Figure 8 shows the C 1*s* main line and satellite structure for C_{70}. Analysis reveals a single feature at 285.3 eV that is 0.2 eV broader than for C_{60}, reflecting the five distinct carbon atoms in the rugby-ball-shaped structure. The satellite features show broad peaks at 2.7, 3.8, and 5.8 eV. Spectra that span a larger energy range reveal distinct peaks due to σ-σ^* transitions at 10 and 13.7 eV, as well as a broad plasmon loss at approximately 28 eV.

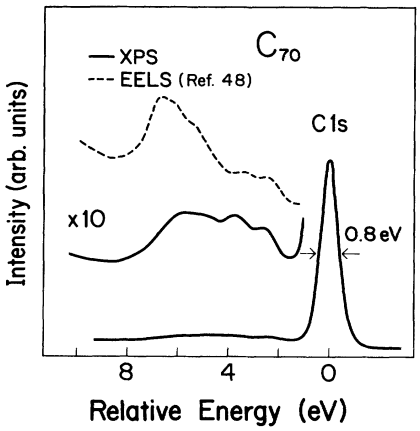

FIG. 8. C 1*s* emission from a C_{70} film grown at 300 K showing a broadened main line relative to C_{60} because of increased inequivalence for the C atoms (binding energy 285.3 eV). The satellite structures reflect the increased spread in the π and π^* energy levels of C_{70} compared to C_{60}. The satellites are due to monopole-allowed (2.7 and 3.8 eV) and dipole-allowed π-π^* excitations. A distinct HOMO-LUMO feature cannot be resolved.

The XPS results indicate the same energy for the high-energy plasmons of C_{60} and C_{70} but the EELS results of Sohmen *et al.*[48] suggest that the plasmon in C_{70} is 1.5 eV lower than in C_{60}. The similarity of the monopole-allowed σ-σ^* shakeup features for C_{60} and C_{70} suggests that the elliptic distortion of C_{70} leaves the energy distribution of σ molecular orbitals with given angular momentum character reasonably intact. The correspondence between features in the photoemission, inverse photoemission, and x-ray absorption spectra for the two molecules supports this.[24,26] A distinct HOMO-LUMO transition could not be resolved for C_{70}, probably because these two levels were broadened in C_{70}, as shown below. Indeed, between the main line and the first defined feature at $\sim$2.7 eV, the intensity remained above the background expected for the main line based on its shape for C_{60}. This probably indicates unresolved loss features from HOMO-LUMO-like transitions.

The peak positions of the broad π-π^* satellite features are in agreement with those observed in EELS, as shown in Fig. 8. These results also compare favorably to the ultraviolet-visible absorption spectrum of C_{70} in solution,[53] suggesting that much of the satellite structure is due to off-site energy losses. The XPS features at 2.7 and 3.8 eV appear strong relative to the corresponding EELS features and, as with C_{60}, this suggests that the C 1s shakeup features had contributions from on-site π-π^* monopole transitions.

Figures 9 and 10 show the distribution of occupied and empty states for C_{70} and K_xC_{70}. For Fig. 9,

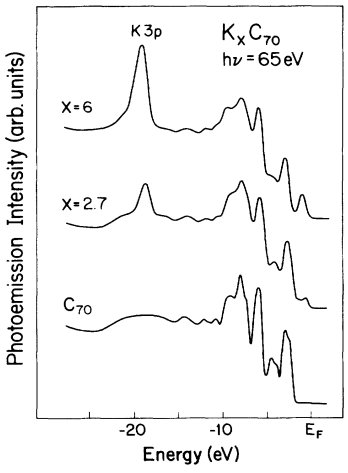

FIG. 9. Valence-band emission from an 80-Å film of C_{70} grown at 300 K and exposed to K. The leading two features are π derived, those from -5 to -10 eV have mixed character, and the deepest features represent σ states. Additional structure in the first two features provides evidence of the energy-level splitting in the C_{70} molecule. The middle spectrum shows a $K_{2.7}C_{70}$ film with emission from partially filled LUMO-derived bands and the K 3p emission 18.3 eV. The top spectrum shows increased emission from the K 3p core level, the filling of LUMO, and a shift of 0.3 eV to lower binding energy as the solid reverts to an insulating state.

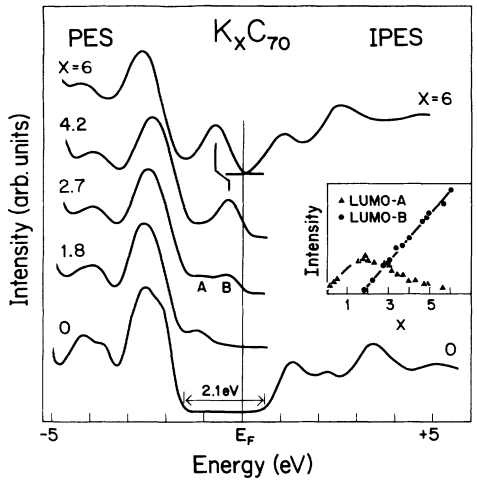

FIG. 10. PES and IPES spectra ($h\nu$=65 eV and E_i=17.25 eV) for K_xC_{70} films prepared at 300 K. The K_0C_{70} spectra show structure within the HOMO and HOMO$-$1 bands. The HOMO-LUMO separation represents the energy necessary to separate an electron and a hole in the solid, not a HOMO-LUMO transition on a single molecule. The $x=1.8$ spectrum shows a split-off band entirely below E_F (LUMO-A). Higher K concentrations produce emission at E_F (LUMO-B) and a shift of the valence features toward E_F. The top spectrum shows complete filling of LUMO. The inset summarizes the intensities of LUMO-A and LUMO-B where LUMO-A increases until $x=1.8$ but then decreases as LUMO-B develops.

stoichiometries of $x=2.7$ and 6 were chosen because they correspond to partially filled and completely filled LUMO bands, based on predictions that the lowest unoccupied bands in C_{70} are derived from a singly degenerate a_1'' level and a doubly degenerate e_1'' level.[64,65] As for C_{60}, the highly symmetric nature of the molecule again assures almost complete spectral features. Even so, comparison to C_{60} shows that the distinct separation between the HOMO and the HOMO$-$1 bands is lost. Resolvable structures within HOMO and HOMO$-$1 reflect the addition of five π states in C_{70} and the lower molecular symmetry. Calculations[55,64,65] for C_{70} predict that the 20 highest electrons lie in HOMO, which is separated from HOMO$-$1 by $\sim$1.5 eV. The calculations show states 5–10 eV below E_F that are of mixed π and σ character and states at higher binding energy that are σ derived. The agreement with experiment is generally quite good but it would be improved by a rigid shift of the σ states to higher binding energy relative to the π states, as for C_{60}.[28] Intriguingly, the experimental line shapes evident in Figs. 9 and 10 for the leading π bands have not been reproduced in the calculations.

Calculations of the energy levels indicate that the first two empty-state features in Fig. 10 contain three states each and are separated by $\sim$1 eV.[64] Other calculated features have highly degenerate peaks $\sim$2.5 and 4.5 eV above LUMO.[64,65] These peaks are in reasonable agreement with those measured with IPES and x-ray absorp-

tion.[24,66] Energy referencing to LUMO should provide reliable relative positions for the higher-lying states, even though the separation between the HOMO and LUMO bands reflects quasiparticle screening (see Sec. VI).

The results of Figs. 9 and 10 show a one to one correspondence between the spectral features of C_{70} and K_6C_{70}, with account taken for broadening. All the valence features shift 0.2 eV to lower binding energy between K_0C_{70} and $K_{2.7}C_{70}$ due to improved screening. There is a shift of 0.3 eV to higher binding energy when the system reached K_6C_{70} and is again insulating. The final shift is analogous to that for C_{60} fullerides but it is smaller because the gap between the LUMO and LUMO+1 levels is smaller.[24,64,65] For C_{70}, light doping did not produce an initial shift, possibly because the contributions due to Fermi-level movement (to higher binding energy) and final-state screening (to lower binding energy) were nearly equal. For K_6C_{70}, the separation between the centers of the two leading bands (formerly HOMO and LUMO) is 1.9 eV. Since the position of these two occupied bands is measured by electron removal, the effects of final-state screening should be the same (Sec. VI). This HOMO-LUMO separation agrees reasonably well with gas phase photoemission results for the negative ion of C_{70},[67] with account taken of the influence of the K ions. In K_6C_{70}, the new HOMO-LUMO gap (top curve Fig. 10) is larger than the separation between the LUMO and LUMO+1 bands of pure C_{70} (0.9 eV, bottom curve Fig. 10), again because measurement of the bands in K_6C_{70} involves electron removal and electron addition.

Perhaps the most remarkable aspect of the photoemission spectra of Fig. 10 is that the initial stage of K incorporation produces a band completely below E_F. This band does not have a counterpart in the K-C_{60} system. For $x \leq 1.8$, a single feature 1.2 eV below E_F is clearly evident and there is no emission near E_F. For $x = 2.7$, two distinct features appeared centered 1.2 and 0.5 eV below E_F, labeled LUMO-A and LUMO-B, and the emission at E_F demonstrates metallic character. This is consistent with resistivity measurements for K_xC_{70}.[3] For $x = 4.2$, there is distinct emission at E_F. The spectrum for K_6C_{70} reveals that the emission intensity of the now-filled LUMO-derived feature is ~ 0.3 times the intensity of the HOMO-derived feature, consistent with predictions of band degeneracies.[64]

The inset in Fig. 10 shows the variation in intensity of LUMO-A and LUMO-B as a function of potassium concentration. Initially, the intensity of LUMO-A increases but it reaches a maximum at $x \cong 1.8$ and then decreases, based on line-shape decomposition of the A and B features. No contributions are evident from LUMO-B until $x \cong 1.8$. The intensity of this feature then increases until the saturated phase is reached. This new doping-dependent electronic structure suggests that there are at least three distinct phases for K_xC_{70}. As the first nonconducting phase is formed, the emission from LUMO-A increases and the sample is probably phase separated into α-C_{70} and a K_2C_{70}-like phase. We speculate that the K_2C_{70} phase has filled tetrahedral sites and the filling may lead to C_{70} molecular alignment in the lattice. The formation of an insulating K_2C_{70}-like phase may indicate that the octahedral sites are so large that a K_3C_{70}-like phase is not energetically favorable. Presumably, the reduced molecular symmetry for C_{70} favors a coupling with the orbitals derived from a_1'' and the splitting off of those levels because they respond to the K potential in tetrahedral sites. A metallic phase, characterized by emission from both LUMO-A and LUMO-B, nucleates and grows at the expense of the phase of lower stoichiometry when the K concentration increases. The presence of the K ions in the lattice may preserve the splitting of the molecular a_1''- and e_1'-derived bands in this phase so that LUMO-A emission persists distinct from LUMO-B. It may be that this metallic phase has K_4C_{70}-like structure with C_{70} molecules in a distorted bcc lattice and K in tetrahedral sites. In contrast, the K_6C_{70} phase is characterized by emission from a single LUMO feature (LUMO-B). K_6C_{70} may be a bcc-based phase with full occupation of tetrahedral sites. The higher symmetry of the bcc K_6C_{70} lattice would reduce the a_1''-e_1'' splitting, giving rise to a single unresolved feature.

The paragraph above has speculated about the phase diagram and crystal structures for K-C_{70} but care should be exercised in using photoemission results to draw definite conclusions until structural studies have been completed. Moreover, the assumption that the low-component phase is K_2C_{70} is based on the appearance of a distinct band derived from a LUMO level that can accommodate two electrons. The alternative would be to suppose that a correlated impuritylike band developed in the gap at low concentration, but resolution of this issue must await detailed structural studies and calculations of the energy levels.

From Fig. 10, it is clear that the emission from the band at the Fermi level for $K_{2.7}$ is spread over ~ 1.5 eV so that the emission intensity at E_F is lower than observed for K_3C_{60}. This and the expected differences in the photon spectra for C_{70} may account for the lack of superconductivity in K-C_{70}. We note that Na_xC_{70} and Cs_xC_{70} show similar valence-band behavior as for K_xC_{70}. Of course this interpretation does not rule out the possibility that there are other differences between fullerenes that will affect the superconducting properties on a more subtle level.

XI. CONCLUSIONS

The results discussed here have revealed the electronic states of C_{60} and C_{70} in solid-state form and the evolution of the electronic states during K incorporation. The combination of photoemission and inverse photoemission shows that the bands are derived largely from molecular levels, with increasing solid-state effects in the empty states. Fulleride formation results in the occupation of the LUMO-derived band by electrons donated from K atoms. We have examined π-π^* and σ-σ^* shakeup features associated with C 1s core excitations, off-site dipole excitations, and molecular plasmons. We have

shown phase separation for K_xC_{60} and K_xC_{70}. Energy shifts in the spectroscopic features have been interpreted in terms of Fermi-level movement and changes in screening with K concentration. Resistivity measurements made in conjunction with photoemission measurements give a dependence on stoichiometry that is indicative of the growth of metallic grains in an insulating medium. These studies also indicate that the sticking coefficient of K changes as the fulleride evolves. Oxidation of the fulleride films shows that K is leached from the fullerene lattice to form surface oxides. The C_{70} results indicate level splitting resulting from the reduced symmetry in the rugby-ball-shaped C_{70} molecule. The appearance of a LUMO-derived feature entirely below the Fermi level in K_xC_{70} demonstrates the existence of a K_xC_{70} phase with no analog in the K_xC_{60} system, undoubtedly reflecting the lower molecular symmetry of C_{70}. We speculate that the absence of superconductivity in K-C_{70} reflects the different electron energy-level spectra as well as the plasmon spectra for C_{70}.

ACKNOWLEDGMENTS

This work was supported by the Office of Naval Research, the National Science Foundation, and the Robert A. Welch Foundation. The synchrotron radiation photoemission studies were conducted at Aladdin, a user facility operated by the University of Wisconsin and funded by the National Science Foundation. We are especially pleased to acknowledge stimulating discussions with J. L. Martins, N. Troullier, and Y. Z. Li. Correspondence and discussions with A. F. Hebard, J. E. Fischer, R. L. Whetten, A Rosén, S. Saito, J. Bernholc, A. A. Lucas, and J. R. Chelikowsky contributed to this work.

[1]H. W. Kroto, J. R. Heath, S. C. O'Brien, R. F. Curl, and R. E. Smalley, Nature (London) **318**, 162 (1985).
[2]W. Krätschmer, L. D. Lamb, K. Fostiropoulos, and D. R. Huffman, Nature (London) **347**, 354 (1990).
[3]R. C. Haddon *et al.*, Nature (London) **350**, 320 (1991).
[4]A. F. Hebard *et al.*, Nature (London) **350**, 600 (1991).
[5]M J. Rosseinsky *et al.*, Phys. Rev. Lett. **66**, 2830 (1991).
[6]K. Holczer, O. Klein, S.-M. Huang, R. B. Kaner, K.-J. Fu, R. L. Whetten, and F. Diederich, Science **252**, 1154 (1991).
[7]P. J. Benning, J. L. Martins, J. H. Weaver, L. P. F. Chibante, and R. E. Smalley, Science **252**, 1417 (1991).
[8]G. K. Wertheim, J. E. Rowe, D. N. E. Buchanan, E. E. Chaban, A. F. Hebard, A. R. Kortan, A. V. Makhija, and R. C. Haddon, Science **252**, 1419 (1991).
[9]C. T. Chen *et al.*, Nature (London) **352**, 603 (1991).
[10]D. M. Poirier, T. R. Ohno, G. H. Kroll, Y. Chen, P. J. Benning, J. H. Weaver, L. P. F. Chibante, and R. E. Smalley, Science **252**, 6464 (1991).
[11]P. W. Stephens, L. Mihaly, P. L. Lee, R. L. Whetten, S.-M. Huang, R. Kaner, F. Deiderich, and K. Holczer, Nature (London) **351**, 632 (1991).
[12]R. M. Fleming, A. P. Ramirez, M. J. Rosseinsky, D. W. Murphy, R. C. Haddon, S. M. Zahurak, and A. V. Makhija, Nature (London) **352**, 787 (1991).
[13]R. M. Fleming *et al.*, Nature (London) **352**, 701 (1991).
[14]O. Zhou *et al.*, Nature (London) **351**, 462 (1991).
[15]K. Tanigaki, T. W. Ebbesen, S. Saito, J. Mizuki, J. S. Tsai, Y. Kubo, and S. Kuroshima, Nature (London) **352**, 222 (1991).
[16]S. P. Kelty, C. C. Chen, and C. M. Lieber, Nature (London) **352**, 223 (1991); C. C. Chen, S. P. Kelty, and C. M. Lieber, Science **252**, 886 (1991).
[17]R. E. Haufler *et al.*, J. Phys. Chem. **94**, 8634 (1990).
[18]STM results are discussed by Y. Z. Li, M. Chander, J. C. Patrin, J. H. Weaver, L. P. F. Chibante, and R. E. Smalley, Science **253**, 429 (1991); **252**, 547 (1991). Atomic force microscopy has been reported by E. J. Snyder *et al.*, Science **253**, 171 (1991). STM studies of monolayer films have been reported by R. J. Wilson *et al.*, Nature (London) **348**, 621 (1990) and J. L. Wragg, J. E. Chamberlain, H. W. White, W. Krätschmer, and D. R. Huffman, *ibid.* **348**, 623 (1990).
[19]D. L. Lichtenberger, K. W. Nebesny, C. D. Ray, D. R. Huffman, and L. D. Lamb, Chem. Phys. Lett. **176**, 203 (1991).
[20]D. L. Lichtenberger, M. E. Jatcko, K. W. Nebesny, C. D. Ray, D. R. Huffman, and L. D. Lamb, in *Clusters and Cluster-Assembled Interfaces,* edited by R. S. Averback, J. Bernholc, and D. L. Nelson, MRS Symposia Proceedings No. 206 (Materials Research Society, Pittsburgh, 1991), p. 673.
[21]J. H. Weaver, J. L. Martins, T. Komeda, Y. Chen, T. R. Ohno, G. H. Kroll, N. Troullier, R. E. Haufler, and R. E. Smalley, Phys. Rev. Lett. **66**, 1741 (1991).
[22]S. Krummacher, S. Cramm, K. Szot, W. Krätschmer, and W. Eberhardt, Phys. Rev. B (to be published).
[23]T. R. Ohno, Y. Chen, S. E. Harvey, G. H. Kroll, J. H. Weaver, R. E. Haufler, and R. E. Smalley, Phys. Rev. B **44**, 13 747 (1991).
[24]M. B. Jost, P. J. Benning, D. M. Poirier, J. H. Weaver, L. P. F. Chibante, and R. E. Smalley, Chem. Phys. Lett. **184**, 423 (1991).
[25]M. B. Jost, N. Troullier, D. M. Poirier, J. L. Martins, J. H. Weaver, L. P. F. Chibante, and R. E. Smalley, Phys. Rev. B **44**, 1966 (1991).
[26]P. A. Heiney, J. E. Fischer, A. R. McGhie, W. J. Romanow, A. M. Denenstein, J. P. McCauley, Jr., and A. B. Smith III, Phys. Rev. Lett. **66**, 2911 (1991).
[27]S. Saito and A. Oshiyama, Phys. Rev. Lett. **66**, 2637 (1991).
[28]N. Troullier and J. L. Martins (unpublished).
[29]J. L. Martins, N. Troullier, and J. H. Weaver, Chem. Phys. Lett. **180**, 457 (1991).
[30]B. Gumhalter, K. Wandelt, and Ph. Avouris, Phys. Rev. B **37**, 8048 (1988).
[31]J. E. Fischer (private communication concerning the phase diagram of K_xC_{60}).
[32]G. P. Kochanski, A. F. Hebard, R. C. Haddon, and A. T. Fiory, Science **255**, 184 (1992); A. F. Hebard (private communication).
[33]A. F. Hebard, R. C. Haddon, R. M. Fleming, and A. R. Kortan, Appl. Phys. Lett. **59**, 2109 (1991).
[34]N. Troullier and J. L. Martins (private communication).
[35]Y. Chen, F. Stepniak, J. H. Weaver, L. P. F. Chibante, and R. E. Smalley (unpublished); T. R. Ohno, G. H. Kroll, J. H. Weaver, L. P. F. Chibante, and R. E. Smalley (unpublished).
[36]T. Ohno, J. H. Weaver, *et al.* (unpublished).

[37]I. Elliot, C. Doyle, and J. D. Andrade, J. Electron Spectrosc. Relat. Phenom. **28**, 303 (1983).
[38]S. Saito and A. Oshiyama, Phys. Rev. Lett. **66**, 2637 (1991).
[39]S. C. Erwin and M. R. Pederson, Phys. Rev. Lett. **67**, 1610 (1991).
[40]E. Sohmen, J. Fink, and W. Krätschmer, Europhys. Lett. **17**, 51 (1991).
[41]G. Gensterblum, J. J. Pireaux, P. A. Thiry, R. Caudano, J. P. Vigneron, Ph. Lambin, A. A. Lucas, and W. Krätschmer, Phys. Rev. Lett. **67**, 2171 (1991); A. A. Lucas (private communication).
[42]D. Nordfors, A. Nilsson, N. Mårtensson, S. Svensson, U. Gelius, and S. Lunell, J. Chem. Phys. **88**, 2630 (1988).
[43]A. Skumanich, Chem. Phys. Lett. **182**, 486 (1991).
[44]S. L. Ren *et al.* (unpublished).
[45]N. Halas (private communication).
[46]M. Braga, S. Larsson, A. Rosén, and A. Volosov, Astron. Astrophys. **245**, 232 (1991).
[47]Y. Saito, H. Shinohara, and A. Ohshita, Jpn. J. Appl. Phys. **30**, 1145 (1991); R. Kuzuo, M. Terauchi, M. Tanaka, Y. Saito, and H. Shinohara, Jpn. J. Appl. Phys. (to be published).
[48]E. Sohmen, J. Fink, R. H. Baughman, and W. Krätschmer (unpublished).
[49]N. Troullier and J. L. Martins (unpublished); N. Troullier, Ph.D. thesis, University of Minnesota, 1991.
[50]M. Cardona and L. Ley, *Photoemission in Solids I,* Topics in Applied Physics Vol. 26 (Springer-Verlag, Berlin, 1979).
[51]P. J. Benning, D. M. Poirier, N. Troullier, J. L. Martins, J. H. Weaver, R. E. Haufler, L. P. F. Chibante, and R. E. Smalley, Phys. Rev. B **44**, 1962 (1991).
[52]H. Ajie *et al.*, J. Phys. Chem. **94**, 8630 (1990).
[53]J. P. Hare, H. W. Kroto, and R. Taylor, Chem. Phys. Lett. **177**, 394 (1991).
[54]Q.-M. Zhang, J.-Y. Yi, and J. Bernholc, Phys. Rev. Lett. **66**, 2633 (1991).
[55]J. W. Mintmire, B. I. Dunlap, D. W. Brenner, R. C. Mowrey, and C. T. White, Phys. Rev. B **43**, 14 281 (1991).
[56]B. Wästberg and A. Rosén, Phys. Scr. **44**, 216 (1991).
[57]F. R. McFeely, S. P. Kowalczyk, L. Ley, R. G. Cavell, R. A. Pollack, and D. A. Shirley, Phys. Rev. B **9**, 5268 (1974).
[58]B. Abeles, *Granular Metal Films,* Applied Solid State Science, Vol. 6 (Academic, New York, 1976), p. 1, and references therein; J. E. Morris, A. Mello, and C. J. Adkins, in *Physical Phenomena in Granular Materials,* edited by T. H. Geballe, D. Sheng, and G. D. Cody, MRS Symposia Proceedings No. 195 (Materials Research Society, Pittsburgh, 1990), p. 181.
[59]S. Kirkpatrick, Rev. Mod. Phys. **45**, 574 (1973).
[60]J. E. Ortega, J. Ferrón, R. Miranda, C. Laubschat, M. Domke, M. Prietsch, and G. Kaindl, Phys. Rev. B **39**, 12 751 (1989); T. Kendelewicz, P. Soukiassian, M. H. Bakshi, Z. Hurych, I. Lindau, and W. E. Spicer, *ibid.* **38**, 7568 (1988).
[61]S. L. Qiu, C. L. Lin, J. Chen, and M. Strongin, J. Vac. Sci. Technol. A **8**, 2595 (1990).
[62]*CRC Handbook of Chemistry and Physics,* 59th ed., edited by C. R. Weast (CRC, Boca Raton, FL, 1979), p. D-74.
[63]G. H. Kroll, P. J. Benning, Y. Chen, T. R. Ohno, and J. H. Weaver, Chem. Phys. Lett. **181**, 113 (1991).
[64]G. E. Scuseria, Chem. Phys. Lett. **180**, 451 (1991).
[65]S. Saito and A. Oshiyama, Phys. Rev. B **44**, 11 532 (1991).
[66]L. J. Terminello, D. K. Shuh, F. J. Himpsel, D. A. Lapiano-Smith, J. Stöhr, D. S. Bethune, and G. Meijer, Chem. Phys. Lett. **182**, 491 (1991).
[67]R. E. Haufler, L.-S. Wang, L. P. F. Chibante, C. Jin, J. J. Conceicao, Y. Chai, and R. E. Smalley, Chem. Phys. Lett. **179**, 449 (1991).